ADVANCED FUNCTIONAL MATERIALS
www.afm-journal.de

Bottom-Up Patterning of Transparent and Conductive Metal–Polymer Composite Hypersurfaces

*Keidy L. Matos, Yerzhan S. Zholdassov, Milan A. Shlain, Antonio R. Cerullo, Mariama Barry, Rajinder S. Deol, Ioannis Kymissis, and Adam B. Braunschweig**

The challenge of fabricating transparent and conductive (T/C) films and patterns for applications in flexible electronics, touch screens, solar cells, and smart windows remains largely unsolved. Traditional fabrication techniques are complex, costly, time-consuming, and struggle to achieve the necessary precision and accuracy over electronic and optical properties. Here, hypersurface photolithography (HP), which integrates microfluidics, a digital micromirror device, and photochemical surface-initiated polymerizations is used to create polymer brush patterns. The high-throughput optimization enabled by HP provides conditions to fabricate patterns composed of cross-linked polymer brushes containing Au-binding 2-vinylpyrrolidine (2VP) groups with precise control over the height and the composition at each pixel. Au nanoparticles (AuNPs) are incorporated into the polymer brush patterns through in situ reduction of Au ions, resulting in T/C composite AuNP/polymer brush patterns. The sheet resistance at 100 mA of a 2VP-AuNP-functionalized patterns on a glass substrate is 0.42 Ω sq^{-1} with 86% transmittance of visible light. Additional patterns demonstrate multiplexing by copatterning rhodamine B functionalized fluorescent polymer brushes and AuNP/polymer brush conductive domains. This work solves the challenge of creating T/C films by forming metal-polymer composites from polymer brush patterns, offering a scalable solution for electronic and optical device development and fabrication.

1. Introduction

There is a growing need for lithography methods that can create transparent and conductive (T/C) patterns for flexible electronics, solar cells, smart windows, touch screens, augmented/virtual reality displays, implants, and sensors, particularly those involving optical detection.[1] In solar cells, these patterns allow light to reach the active layer while providing a mechanism for collecting and transporting charge carriers.[2] In touch screens, tablets, smartphones, and interactive kiosks, T/C patterns provide pathways for charge transport while maintaining the screen's clarity and responsiveness.[3–5] These patterns ensure that electrical signals can pass through without disrupting the visual display, while still allowing for smooth and accurate touch sensitivity. Furthermore, their flexibility and durability are essential for withstanding repeated use and ensuring long-term device performance, even in flexible or foldable screens. Optical sensors that conform to the human body require flexible and stretchable T/C materials to maintain both electrical conductivity and optical functionality during movement.[6] These applications often require that the T/C patterns are applied onto substrates, including glass, plastics, or textiles, which are not substrates typical for conventional microfabrication approaches.[7] So, to fabricate the next generation of electronic, wearable devices, there is a pressing need for lithography methods that can prepare T/C patterns on diverse substrates.

K. L. Matos, Y. S. Zholdassov, M. A. Shlain, A. R. Cerullo, M. Barry, A. B. Braunschweig
Advanced Science Research Center
Graduate Center
City University of New York
85, St. Nicholas Terrace, New York, NY 10031, USA
E-mail: abraunschweig@gc.cuny.edu

K. L. Matos, Y. S. Zholdassov, M. A. Shlain, A. R. Cerullo, A. B. Braunschweig
Department of Chemistry
Hunter College
695 Park Avenue, New York, NY 10065, USA

K. L. Matos, Y. S. Zholdassov, M. A. Shlain, A. B. Braunschweig
PhD Program in Chemistry
Graduate Center
City University of New York
365 5th, Avenue, New York, NY 10016, USA

A. R. Cerullo, A. B. Braunschweig
PhD Program in Biochemistry
Graduate Center
City University of New York
365 5th, Avenue, New York, NY 10016, USA

R. S. Deol, I. Kymissis
Department of Electrical Engineering
Columbia University
New York, NY 10027, USA

The ORCID identification number(s) for the author(s) of this article can be found under https://doi.org/10.1002/adfm.202502414

DOI: 10.1002/adfm.202502414

Despite the growing need, the preparation of T/C patterns and in turn the widespread adoption of devices that incorporate such patterns, faces several challenges related to substrate-chemistry compatibility, difficulty in creating surfaces that combine soft and hard materials,[8] and the slow throughput of the design-test-optimization cycle.[9] T/C patterns are produced most frequently using top-down techniques like sputtering or chemical vapor deposition (CVD), and solution-based methods such as spin and spray coating.[10] CVD involves depositing a thin metallic film through a mask onto a substrate, but this process often requires high temperatures and vacuum conditions that may be incompatible with soft materials or certain substrates.[11] The spin coating of thin films is scalable,[12] but involves additional steps such as masking or surface modification to create patterns. Combining these methods to tailor the electrical properties within a pattern poses significant challenges, particularly when integrating soft (organic, polymeric, and biological) and hard (inorganic and metallic) materials. This integration can lead to poor adhesion,[13] cracking,[14] or delamination,[15] adversely affecting the film's conductivity and mechanical properties. Such issues are especially critical for applications requiring biotic and abiotic integration, like bioelectronics or wearable devices, where flexibility and biocompatibility are crucial.[16] Alternatively, bottom-up approaches build structures from smaller components through self-assembly or controlled deposition. These methods, such as templated self-assembly of nanoparticles (NPs), offer nanoscale precision without extensive material removal and allow for tailored material integration and patterning. However, many bottom-up techniques require further optimization to achieve high throughput and scalability over large areas. Moreover, these methods involve multiple steps and specialized equipment, often necessitating clean room environments, which limits accessibility. Finally, the low-throughput of preparing and characterizing these films, often yielding only a few samples per day or per processing sequence, hinders the testing and optimization cycle involved in the development of new film and processing conditions.[9] Therefore, there is a continued need for lithographic methods that can print T/C patterns, accommodate different materials, and can print over large (>1 cm^2) areas with high throughput.

Many of these drawbacks could be overcome with the use of patterned polymer brushes.[17] This approach involves grafting polymers onto or from a surface and then modifying the resulting polymer brushes with conductive elements, such as gold nanoparticles (AuNPs),[18] or alternatively, the polymer brushes themselves are conductive.[19] By leveraging techniques such as surface-initiated photopolymerization (SIP), patterns can be fabricated with sub-3 micrometer precision over large areas while accommodating various materials within the pattern design.[20–22] The advantages of using polymer brushes include the ability to create a uniform, defect-free coatings and the versatility to modify surface properties[20] by adjusting the polymer composition and brush height, *h*. In addition, the brushes can be grafted covalently to the surfaces, ensuring a strong attachment to the substrate.

To date, significant progress has been made in creating conductive polymer brush patterns using various photolithographic techniques.[23] However, one of the significant challenges with these patterns, particularly when polymer brushes are involved, is achieving sheet resistance (R_s) below 10 Ω sq^{-1} for high-performance applications, such as optical detection systems or solar cells, and 10 to 100 Ω sq^{-1} required for uses in flexible electronics, touch screens, and displays.[24] For example, researchers have used SIP to create conductive polymer brushes, such as poly(monomethyl itaconate) (PMMI) grafted multi-layer graphene oxide (PMMI-*g*-GO) and poly(4-vinylaniline) nanospheres, and in doing so have achieved materials with electrical conductivity as high as 5.04 S m^{-1} (R_s = 1.98 × 10^5 Ω sq^{-1}, for a 1 μm thick layer)[25] and 3 × 10^{-1} S cm^{-1} (R_s = 8.12 × 10^5 Ω sq^{-1}, for a shell thickness of 41 nm),[26] respectively. Another significant advancement is block copolymer lithography, which combines the self-assembly of block copolymers with photolithographic techniques to create nanoscale patterns.[27] This approach has been employed to produce highly ordered, periodic patterns of polymer brushes with conductive domains. Notably, the incorporation of conductive polymers like poly(3-hexylthiophene) (P3HT) has demonstrated good electrical performance.[28] P3HT's crystallinity helps form efficient charge transport pathways, even at low concentrations (as low as 3 wt%), without degrading the device's performance. However, this crystallinity renders it difficult to achieve desirable transparency because of light scattering, the challenge of uniform integration when mismatched surface interactions may occur, and the inability to immobilize into arbitrary, multiplexed patterns because of the limitations of the lithographic methods.

Organic polymer brushes themselves often have unsatisfactory conductivity for electronic applications because of the insulating nature of most organic polymer matrices.[29] Previously this challenge has been addressed by incorporating conductive additives into patterns, including metal NPs,[30] such as AuNPs,[18,31] CuNPs,[32] and AgNPs,[33] or carbon nanotubes,[34] Ag nanowires,[4,35]or conductive polymers[36] in an attempt to increase conductivity. For example, Ag nanowire additives can achieve sheet resistances of 10 Ω sq^{-1} with over 90% transparency,[37] making them one of the best performers for applications requiring high conductivity, flexibility, and transparency. Additionally, metal NP–polymer composite films have demonstrated excellent conductivity when structured as multilayered architectures. Polymeric materials serve as both substrates and binders for metal NPs, allowing for precise structural control and enhanced conductivity.[38] For instance, a multilayer polymer-metal film has been reported to achieve a sheet resistance of 5 Ω sq^{-1} with 78% transmittance,[39] while an oxide/metal/polymer composite exhibited 15.1 Ω sq^{-1} with 87.4% transmittance.[40] These results demonstrate that incorporating polymer-metal hybrid structures can lead to highly conductive films while maintaining excellent optical transparency. However, these approaches have often struggled with achieving uniform distribution and integration of conductive materials, highlighting the need for more advanced and precise fabrication techniques .[41] AuNPs, known for their exceptional electrical conductivity, chemical stability, and biocompatibility, are particularly promising candidates for enhancing the conductivity of these polymer brush films.[42] In sputtered Au films, sheet resistivity as low as ≈10^{-5} Ω cm (10 Ω sq^{-1})[43] have been reported for continuous films with thicknesses around 10 nm, and this value is only one order of magnitude higher than that of the resistivity of bulk gold, 2.44 × 10^{-6} Ω cm (2.44 Ω sq^{-1})[44] at that thickness, demonstrating that such films could offer attractive conductivity

if further optimized. The challenge of achieving AuNP/polymer brush composites with low R_s is that precise control over the size, shape, and surface chemistry of the NPs is necessary to ensure integration in sufficiently high concentrations to achieve desirable conductivity (<1 Ω sq^{-1}) for high-performance applications. Furthermore, the high concentrations of AuNPs necessary for low R_s can compromise the film's transparency,[45] limiting their effectiveness in applications where both transparency and conductivity are crucial. Additionally, the low throughput of current fabrication processes hinders the synergistic exploration of the relationships between polymer architecture, AuNP integration, conductivity, and transparency required to optimize these fabrication processes. Until these problems are solved, the promise of AuNP/polymer–brush composites as T/C elements in electronic circuits will remain unrealized.

Here, we address the challenges of creating T/C AuNP/polymer brush composite patterns with R_s <1 Ω sq^{-1} by combining hypersurface photolithography (HP),[46] the grafted-to/grafted-from radical photopolymerization (GTGFRP),[47] and bottom-up, templated AuNP self-assembly. A polymer brush hypersurface refers to a printed structure where multiple independent properties of each voxel can be precisely controlled.[9,48] Polymer brushes with Au-binding 2-vinyl pyrrolidine (2VP) groups[49] were grafted from Si/SiO_2 and glass surfaces. These structures were then incubated in a solution of Au ions, and subsequently reduced to create AuNP/polymer–brush composite patterns. The ability of HP to test polymer brush growth conditions with ultra-high throughput, enabling the screening of hundreds-to-thousands of conditions in a single experiment,[9] was used to optimize SIP conditions, so relationships between polymer architecture, metal incubation and reduction, conductivity, and transparency could be explored systematically. The result is patterns with micrometer-scale line widths and R_s as low as 0.42 Ω sq^{-1} on both silicon wafers and glass substrates, and whose conductance is independent of the underlying surface. Additional multiplexed patterns were created by copatterning AuNP/polymer brush composites and fluorescent polymer brushes containing Rhodamine B methacrylate monomers onto the same substrate. This approach enabled the successful production of multiplexed, arbitrary patterns without the need for masks, while effectively blending soft and hard materials within the same structure. This significantly advances the field of bottom-up, mask-free lithography by enabling rapid, high-throughput testing and optimization of AuNP/polymer brush composites, paving the way for the development of high-performance, multiplexed, and T/C patterns for various optical and electronic applications.

2. Results and Discussions

2.1. Patterning Au-Binding Polymer Brushes with Independent Control over Height at Each Pixel

HP[22,46–48,50] (Figure 1) combines a 405 nm LED, and a digital micromirror device (DMD) with ≈700 000 individually addressable mirrors, and a fluid cell, where SIPs occur, with integrated microfluidic control of reagents to create multiplexed polymer brush patterns.[9] By coordinating the microfluidics with the delivery of light, the h, the chemical composition at each pixel (a pixel corresponding to an individual mirror in the DMD), or the reaction condition at each pixel can be controlled independently. As a result, thousands of different reaction conditions can be tested on each printed substrate, allowing for the rapid screening of reaction conditions and high-throughput optimization of surface chemistry. To this end, HP has been used to study the kinetics of grafted-from photopolymerizations,[9] create stimuli-responsive hypersurfaces,[46,48] and create biosensors with attomolar sensitivity.[47] Here, HP was first used to study the growth rates of 2VP-containing polymer brushes grown by the GTGFRP. The GTGFRP is a living, photochemically driven thiol-initiated radical photopolymerization,[9,51] where branched polymer brushes composed of ethylene glycol dimethacrylate (EGDMA) and pentaerythritol tetrakis(3-mercaptopropionate) (PETT) monomers are grafted from a thiol-terminated substrate. By adding molecules with terminal alkenes to the reaction solution, functional groups are incorporated into the growing polymer brush via covalent C—S bonds. In this process, 2VP is introduced into the printing solution as part of the polymerization and as a result, is incorporated throughout the polymer brush structure. This results in 2VP-EGDMA-PETT polymer brushes that are immobilized covalently onto the surface and with the ability to bind metal ions throughout.[52]

The high-throughput screening capabilities of HP were relied upon to systematically explore the effects of [2VP], light intensity, and irradiation time, t, on the growth rate of 2VP-EGDMA-PETT polymer brushes, with 576 conditions tested using the same pattern. To print the polymer brush patterns (Figure 2A), a solution containing EGDMA, PETT, 2VP, and the photoinitiator diphenyl(2,4,6-trimethylbenzoyl)phosphine oxide (TPO) in DMSO was prepared under inert atmosphere and introduced into the fluid cell of the HP printer. The mixture was then irradiated with 4 μm x 500 μm line patterns of 405 nm light, where each of the 12 lines within a pattern was irradiated at t from 58 to 80 min. Following the printing, the surfaces were washed with EtOH and air-dried to remove any physiosorbed monomers. The presence of the printed patterns was confirmed using optical microscopy (Figure 2B). The h of each feature was measured using profilometry (Figure 2C), and the ability to print 12 patterns of 12 lines on each surface produced high-fidelity datasets so variance between lines on different patterns could be measured accurately. Figure S4 (Supporting Information) shows that the growth rate of the 2VP-EGDMA-PETT polymer brushes increases as [2VP] increases. Figure 2C shows that at [2VP] = 500 mM, the h of these polymer brushes can be varied controllably from 8.0 ± 2.5 to 3800 ± 8.7 nm. The polymerization process is influenced by multiple parameters, including [monomer], [photoinitiator], light intensity, and t. And although >9000 conditions were tested, the work here only samples a fraction of the total parameter space for this reaction, and we do not yet fully understand what fundamentally limits the maximum achievable h. To confirm the presence of 2VP-groups within the polymer brush features, X-ray photoelectron spectroscopy (XPS) was performed on a 2VP-EGDMA-PETT polymer brush substrate and compared to a substrate with EGDMA-PETT polymer brushes. A significant N1s signal is observed with the substrate which contained the 2VP-EGDMA-PETT polymer brushes (Figure 2D), which is consistent with the proposed chemical structures of the polymers, but no such peak was observed for the EGDMA-PETT brushes that

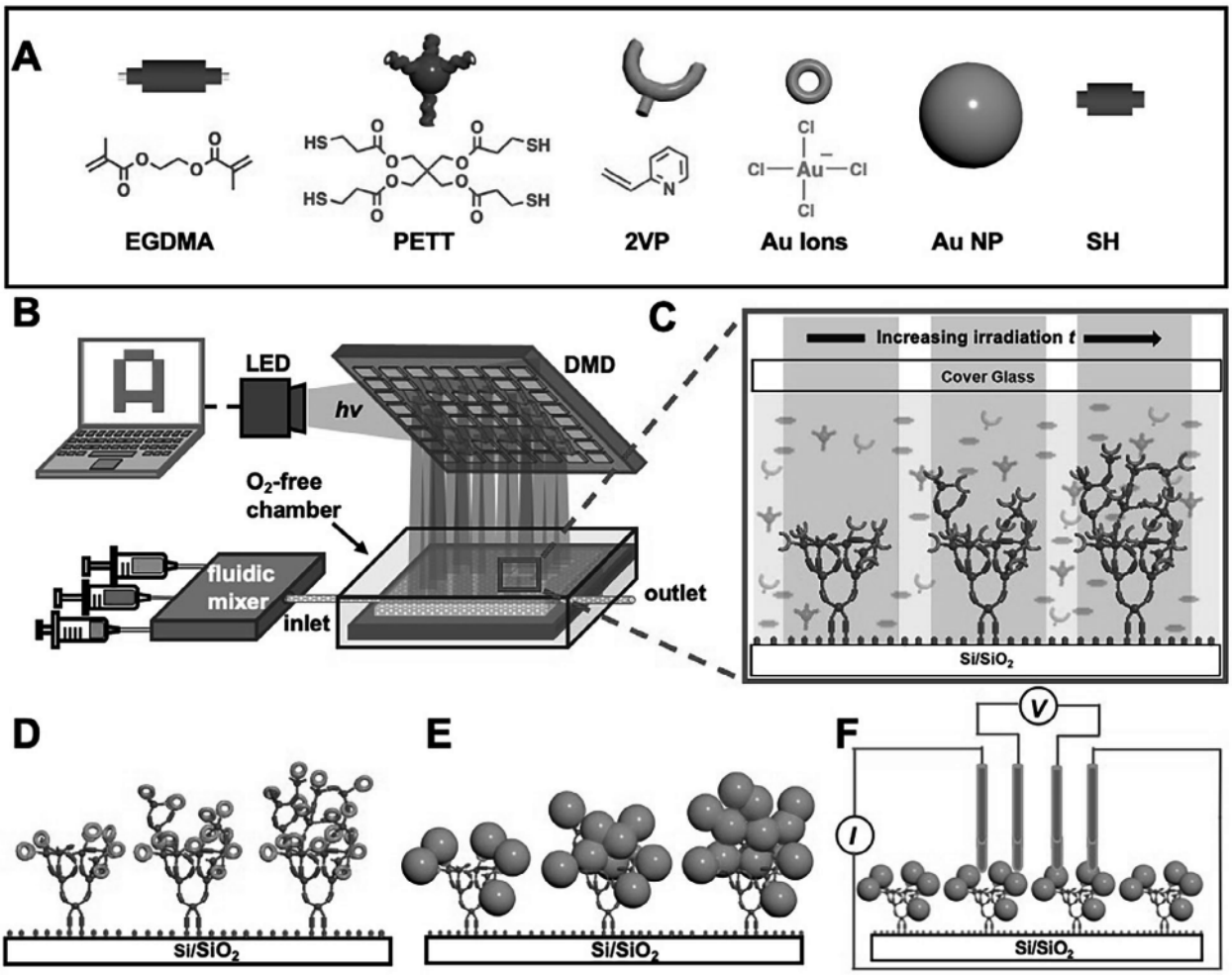

Figure 1. A) Elements involved in the bottom-up printing of T/C wires using the grafted-to/grafted-from radical photopolymerization (GTGFRP). B) The hypersurface photolithography (HP) printer used for surface patterning combines a digital micromirror device (DMD), a microfluidics-enabled fluid cell, and a reactive surface. C) Patterned polymer brushes growing from a thiol-terminated Si/SiO_2 surface by consuming monomers in solution upon exposure to light (purple lines). As the irradiation time, *t*, increases, the height, *h*, of the polymer brushes increases. D) 2VP-EGDMA-PETT polymer brushes on thiol-terminated Si/SiO_2 surface bind Au ions. E) Upon reduction of Au-ions in (D) with $NaBH_4$, gold nanoparticles (AuNPs) form. F) Measuring R_s of polymer-brush patterns shown in (E) using a four-point probe.

lack N, indicating that the incorporation of 2VP into the polymer brushes was successful. Time-of-flight secondary ion mass spectrometry of the 2VP-EGDMA-PETT polymer brushes was taken and compared to that of the EGDMA-PETT polymer brushes (Figure 2E). The mass spectra show that the 2VP-EGDMA-PETT surface had peaks with *m/z* corresponding to the aniline groups of 2VP, which were not present in the spectra of the EGDMA-PETT samples. These results demonstrate the ability to control precisely the *h* and chemical composition of the polymer brushes at each feature in the patterns.

2.2. Au Ion Binding and In Situ Reduction to Form AuNP/Polymer Brush Composites

To demonstrate the selective binding of AuNPs to the 2VP-EGDMA-PETT polymer brushes, two approaches to incorporating AuNPs into the brushes were tested: incubating pre-synthesized AuNPs with a surface that had been patterned with 2VP-EGDMA-PETT, and the in situ generation of AuNPs by reduction of Au ions bound to the 2VP groups on the patterned 2VP-EGDMA-PETT polymer brushes. For the former method, EGDMA-PETT polymer brushes and 2VP-EGDMA-PETT polymer brushes were printed on separate substrates, and these substrates were incubated for 1 h in a solution of pre-synthesized AuNPs (≈30 nm diameter). For the latter method, the polymer brush-modified substrates were first incubated in 0.1 mM $HAuCl_4$ (aq) for 1 h and then reduced with 1 mM $NaBH_4$ (aq) for 1 h. These samples were analyzed with XPS to detect the presence of AuNPs onto the different polymers. Results from XPS analysis showed no significant binding of Au to the EGDMA-PETT polymer brushes, irrespective of the incubation method (Figures S9 and S10, Supporting Information). With in situ AuNP formation the 2VP-EGDMA-PETT polymer brushes showed distinct Au4f peaks at 85 eV, with peak intensity of 410 a.u., confirming Au binding (Figures S11 and S12, Supporting Information).

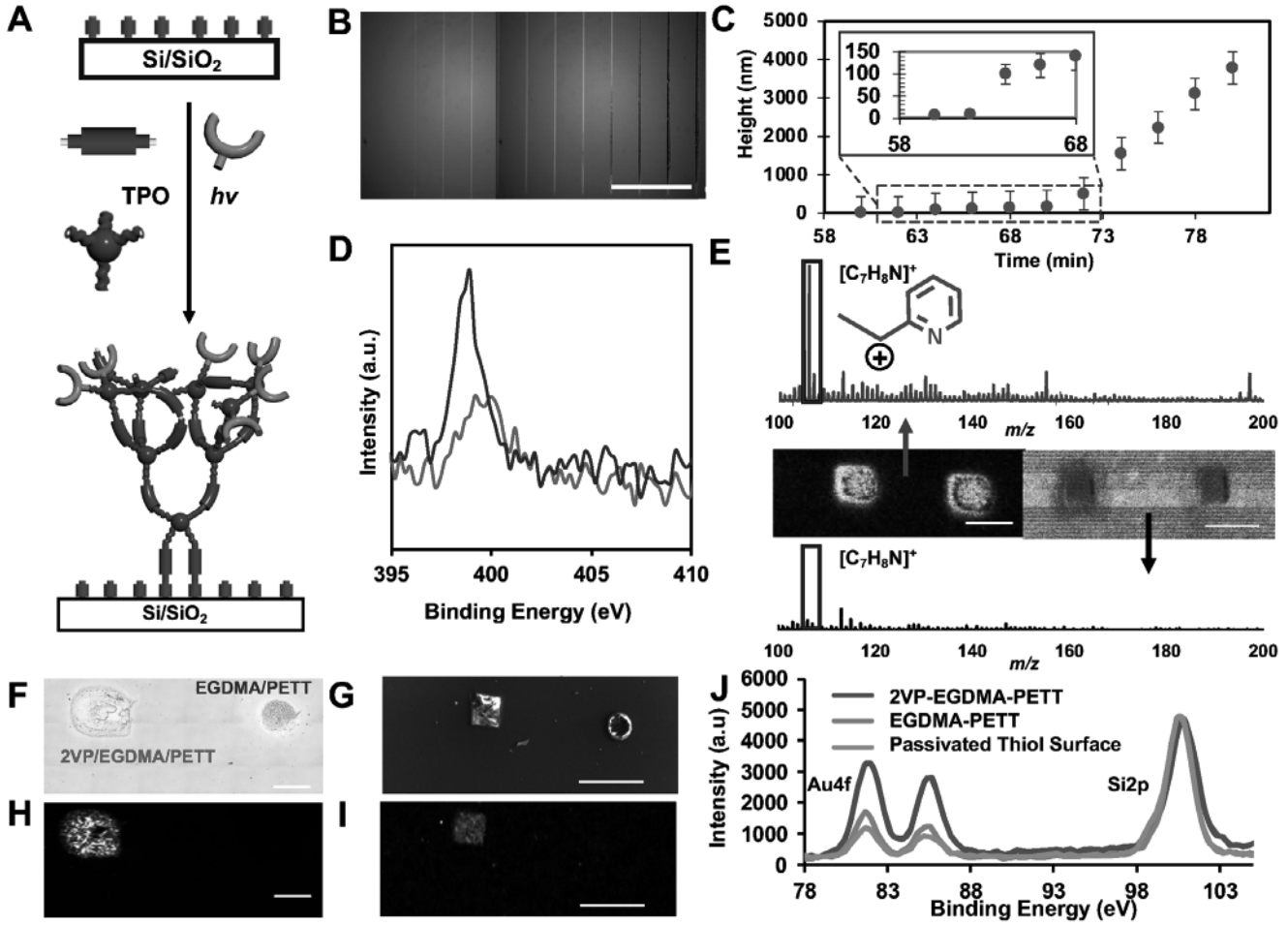

Figure 2. A) Preparation of 2VP-EGDMA-PETT polymer brushes via the GTGFRP. B) Optical image of 2VP-EGDMA-PETT polymer brushes patterned onto a thiol-functionalized Si/SiO_2 wafer. Scale bar is 200 µm. C) *h* versus *t* plot of the brushes shown in (B), as determined by profilometry. Heights are reported as the average of 3 features printed at the same *t*, and all error bars are reported as one standard deviation from the mean. D) XPS spectrum (N1s) of polymer brush patterns 2VP-EGDMA-PETT polymer brushes (blue) ([2VP] = 500 mM; [EGDMA] = 1300 mM; [TPO] = 1 mM; light intensity = 2.53 mW mm^{-2}; [PETT] = 100 mM) and EGDMA-PETT polymer brush features, which were printed without 2VP ([EGDMA] = 1300 mM; [TPO] = 1 mM; light intensity = 2.53 mW mm^{-2}; [PETT] = 100 mM). E) Bottom: Time-of-flight secondary ion mass spectrometry spectra of (bottom) EGDMA-PETT polymer brush features ([EGDMA] = 1300 mM; [TPO] = 1 mM; light intensity = 2.53 mW mm^{-2}; [PETT] = 100 mM). Bottom: 2VP-EGDMA-PETT polymer brush features ([2VP] = 500 mM; [EGDMA] = 1300 mM; [TPO] = 1 mM; light intensity = 2.53 mW mm^{-2}; [PETT] = 100 mM). Black boxes are at $m/z = 106.0$, corresponding to the fragment $[C_7H_8N]^+$. Center: Total ion images are shown. Scale bars are 100 µm. F) Optical image of pattern containing 2VP-EGDMA-PETT polymer brushes (squares) and EGDMA-PETT polymer brushes (circle) that do not contain 2VP and cannot bind Au ions. Scale bars are 100 µm. G) SEM image of polymer brushes in (F). Scale bars are 250 µm. H) Raman spectroscopy map of polymer brushes in (F). Scale bars are 100 µm. I) SEM/EDS image of Au Mα1 of the polymer brushes in (F). Scale bars are 250 µm. J) XPS spectrum of Au4f of the passivated 2VP-EGDMA-PETT polymer brushes, a passivated thiol-functionalized surface, and MA-passivated surfaces with EGDMA-PETT polymer brushes that do not contain the 2VP groups.

The surfaces incubated with AuNPs also displayed Au4f peaks in their XPS spectra, but with a lower peak intensity of 320 a.u. We speculate that this lower intensity is because of the inability of AuNPs to migrate through the pores of the polymer brush network and bind 2VP groups within the pillars. To maximize AuNP incorporation with the in situ reduction, the concentration of $HAuCl_4$ was increased to 1 mM, and the $NaBH_4$ concentration was increased to 10 mM, which significantly increased the Au4f peak intensities within the 2VP-EGDMA-PETT samples to 3000 a.u. To prevent non-specific Au binding to unreacted thiols on EGDMA-PETT polymer brushes or on the thiol-terminated substrate, the unreacted thiol groups were passivated by incubation of the patterned substrates in a solution of maleic anhydride (MA) for 30 min.[53] After passivation, XPS analysis revealed reduced Au4f peak intensities for the EGDMA-PETT polymer brushes and the thiol-terminated substrates. However, the 2VP-EGDMA-PETT polymer brushes retained high Au4f XPs intensities (3000 a.u.), signifying substantial Au-binding (Figure S14, Supporting Information). This increase in Au4F intensity of 2VP-EGDMA-PETT compared to EGDMA-PETT brushes suggests that the 2VP units play a crucial role in facilitating Au binding, and that the MA treatment effectively minimizes non-specific binding to unreacted thiol groups within the brushes and on unpatterned regions of the substrate. We anticipate that

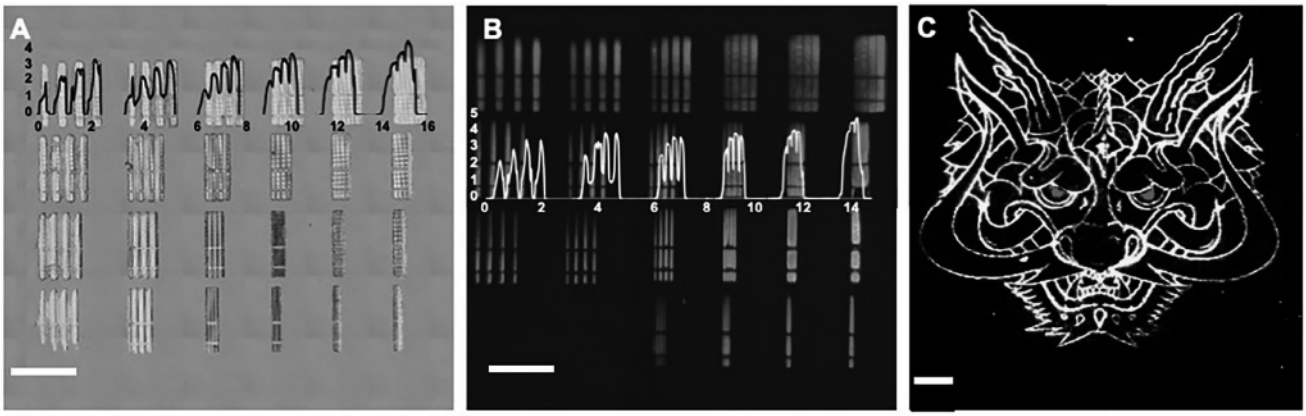

Figure 3. A) Optical image of 2VP-EGDMA-PETT polymer brush lithography test pattern with profilometry trace indicating the *h* of each feature. The *x*-axis units are in mm and *y*-axis units are in µm. Scale bars are 900 µm. B) Fluorescent micrograph of rhodamine B methacrylate (RMA) functionalized polymer brush lithography test pattern with profilometry trace indicating the *h* of each feature on the corresponding row. The *x*-axis units are in mm and *y*-axis units are in µm. Scale bars are 900 µm. C) Fire dragon with glowing red eyes. Raman map of a 2VP-EGDMA-PETT and RMA-EGDMA-PETT multiplexed polymer brush pattern. Area scans were taken with 532 nm lasers and 633 nm laser for measuring Au and RMA peaks, respectively, and the image of the fire dragon is produced by overlaying the two Raman maps. Yellow shows peak intensities at 310–350 cm^{-1} (λ_{ex} = 532 nm). Red shows peak intensities at 1400–1460 cm^{-1} (λ_{ex} = 633 nm). Individual Raman maps for 310–350 cm^{-1} (λ_{ex} = 532 nm) and 1400–1460 cm^{-1} (λ_{ex} = 633 nm) are provided in Figures S15 and S17 (Supporting Information), respectively. Scale bar is 200 µm.

varying AuNP size and density could affect conductivity and transparency.

To further demonstrate the selective binding of Au to the 2VP-EGDMA-PETT polymer brushes under the in situ AuNP formation conditions, a multiplexed pattern was prepared, where the 2VP-EGDMA-PETT polymer brushes were printed into squares and the EGDMA-PETT polymer brushes were printed into circles (Figure 2F) on the same substrate. This multiplexed substrate was passivated with MA followed by a 1 h incubation in 1 mM $HAuCl_4$ solution and then reduced with 10 mM $NaBH_4$(aq) for 1 h. The substrates were analyzed by Raman mapping to confirm that the Au is bound within the polymer brush pattern by the presence of characteristic Au peaks[54] at 310–350 cm^{-1} (λ_{ex} = 532 nm) (Figure 2H). This Raman map, along with the energy-dispersive X-ray spectroscopy (EDS) map of the Au Mα1 intensity (Figure 2I), confirms that the 2VP-EGDMA-PETT polymer brush regions selectively contained bound Au. The absence of Raman or EDS intensity corresponding to Au in the EGDMA-PETT circles further confirms that the Au ions selectively bind to the 2VP-EGDMA-PETT polymer brushes containing 2VP groups. XPS analyses of these surfaces also confirm the selective binding of Au to the 2VP-EGDMA-PETT polymer brushes (Figure 2J), with the 2VP-EGDMA-PETT polymer brushes showing a much higher Au4f intensity than that of the EGDMA-PETT brushes or the MA-passivated regions of the thiol-terminated SiO_2 surface.

2.3. Multiplexed Patterning of Au-Binding and Fluorescent Polymer Brushes

Test patterns in photolithography are prepared so that the widths and roughness of features prepared under different conditions can guide the production of patterns with certain feature dimensions.[55] Here, a test pattern consisting of lines that vary in thickness from 5 to 70 µm, which are assembled in groups of 4, where in each descending row the spacing between lines varies from 100 to 5 µm, was prepared (Figure S6, Supporting Information). The first test pattern was printed using 2VP-EGDMA-PETT polymer brushes, and another test pattern was printed with polymer brushes that contain the fluorescent monomer Rhodamine B methacrylate (RMA) by adding RMA to EGDMA and PETT during the photopolymerization, resulting in RMA-EGDMA-PETT polymer brushes.[46,48] The profilometry trace of the 2VP-EGDMA-PETT polymer brush test pattern showed that as the spacing between the lines decreases, the *h* of the brushes increase, and the polymer features merge when spacing is <10 µm (Figure 3A). The RMA-EGDMA-PETT polymer brush pattern showed similar results, where, as the spacing between the lines decreased, the polymer brushes grew taller and merged (Figure 3B). From these experiments, it was concluded that line widths ranging from 5 µm to 70 µm could be printed, and that the distance between non-intersecting lines should be ≥ 10 µm to prevent feature merging. While the resolution is influenced by instrumental factors, such as the size of the mirrors in the DMD and the magnification of the lenses in the HP printer, it is also possible that chemical properties, including polymer diffusion and crosslinking kinetics, influence pattern resolution. Future studies will explore the interplay between optical resolution and polymerization dynamics to determine the fundamental resolution limits of this system.

Using the guidance from the test patterns, a multiplexed print consisting of 2VP-EGDMA-PETT and RMA-EGDMA-PETT patterned into a fire dragon with fluorescent red eyes was designed (Figures S18 and S19, Supporting Information and Figure 3C). Following printing, the substrate was incubated with $AuCl_4$(aq) ions (1 mM), reduced with $NaBH_4$(aq) (10 mM), washed, and analyzed by profilometry, optical microscopy, and Raman mapping. Two different Raman spectroscopy maps of this pattern were taken, one with a 532 nm laser to observe the Au peaks

(310–350 cm^{-1}) within the printed pattern (shown in yellow) and another with 633 nm to detect the RMA (1400–1460 cm^{-1}) (shown in red) within the print. These two different maps were then merged to complete the full image of the fire dragon. RMA peaks were only observed on the eyes (RMA-EGDMA-PETT brushes) and Au peaks were only observed on the lines forming the face (2VP-EGDMA-PETT brushes). The resulting print demonstrates our ability to successfully produce multiplexed, arbitrary patterns, mask-free, and without necessitating cleanroom conditions, while blending soft and hard materials on the same surface and with precisely defined relative positions. This multiplexed print is made possible by the advantages of high-throughput optimization, material diversity, and pattern flexibility offered by combining HP and the GTGFRP.

2.4. Transparency and Conductivity of AuNP/Polymer Brush Composites

To analyze the transparency of our Au polymer brush samples, 4 × 3.5 mm rectangular patterns of 2VP-EGDMA-PETT were printed on a thiol-functionalized glass slide. This large pattern was selected to ensure accurate measurement of transparency across the sample. This sample was then passivated with MA, incubated in 1 mM $HAuCl_4$(aq), and reduced with 10 mM $NaBH_4$(aq) to form the AuNP/polymer brush composites. While no pattern is visible by optical microscopy (**Figure 4A**), a Raman spectroscopy map of the Au intensities (310–350 cm^{-1}, λ_{ex} = 532 nm) confirmed the presence of the AuNPs in the pattern (Figure 4B). SEM images of this pattern were taken to visualize the size of the AuNPs (Figure 4C), and ImageJ image processing software[56] was used to measure the size of the AuNPs on the surface (Table S2 and Figures S25 and S26, Supporting Information). These images indicated that the average diameter of the AuNPs was 79 ± 17 nm, where the error is reported as one standard deviation from the mean. The UV-Vis absorbance data supports the size determination of these AuNPs based on the peak at λ_{max} = 580 nm that emerges upon reduction with $NaBH_4$(aq) (Figure 4D, inset), which corresponds to AuNPs with diameters of 80 nm according to Mie theory.[57] Transmission measurements (Figure 4E) show an average transmittance of 86% over the wavelength range of 500–800 nm.

To test the conductivity of these polymer–AuNP composites, a 4-point probe device was designed and fabricated. The device consists of 4 metal pogo pins of 16 mm length with a pin-to-pin spacing of 2.5 mm (Figure S27, Supporting Information). The pins were connected and wired using a GH 1.25 mm 4-pin housing, which was then attached to an Agilent B2901A current source and an Agilent 34405A multimeter. To test the accuracy of this device, three different samples of known conductivity were tested, including samples of Ag paint, Cu tape, and an SiO_2 wafer coated in 50 nm of Au. The R_s of these three materials were consistent with their known conductivities—Ag being the most conductive, followed by Cu, and then Au (Figure 4F,G and Table S4, Supporting Information). Also, the following non-conductive samples were tested, a glass substrate, an Si/SiO_2 substrate, and 2VP-EGDMA-PETT polymer brush samples, and their R_s values exceeded the maximum sensitivity of the detector of 450 Ω sq^{-1}. The AuNP/2VP-EGDMA-PETT polymer brush samples were prepared on two insulating substrates, thiol-terminated SiO_2 wafers with 500 nm thermal oxide and transparent thiol-terminated glass slides. On the SiO_2 substrate, AuNP/2VP-EGDMA-PETT polymer brushes features were prepared with dimensions of 8 mm × 3.5 mm to ensure contact with all 4 pins. Measurements were taken on this Au-ion/2VP-EGDMA-PETT (2VP Au Ions SiO_2) samples (not reduced with $NaBH_4$) to examine whether the reduction from Au ions to AuNPs affected conductivity. The R_s measured for a 100 mA input of current on the AuNP/2VP-EGDMA-PETT (2VP AuNP SiO_2) polymer brushes sample was 0.38 ± 0.02 Ω sq^{-1}, whereas for the Au-ion/2VP-EGDMA-PETT polymer brush sample the R_s measured was 0.69 ± 0.07 Ω sq^{-1}. A sample of AuNP/2VP-EGDMA-PETT (2VP AuNP Glass) on a glass cover slide was taken, the R_s of 0.42 ± 0.01 Ω sq^{-1} at 100 mA input showed to be very consistent with that of the AuNP/2VP-EGDMA-PETT on SiO_2 (Figure 4G). For comparison, the sheet resistance of bulk Au for a 1 µm thick sample is 0.0244 Ω sq^{-1}.[44] While this study focuses primarily on the fabrication and characterization of T/C polymer-AuNP composites, assessing their long-term stability is essential for practical implementation. To evaluate durability, we conducted 250 current input cycles and observed that the films surpassed a sheet resistance of 1 Ω sq^{-1} after 148 cycles. The resistance stabilized after 230 cycles, remaining consistent at 1.34 Ω sq^{-1} (Figure S28, Supporting Information). Future work will further investigate the stability of these materials under varied environmental conditions, including humidity, thermal cycling, and mechanical strain.

The results obtained from the 2VP-EGDMA-PETT-Au polymer brush samples highlight a significant improvement in conductivity when compared to conventional conductive polymers, like (poly(3,4-ethylenedioxythiophene) polystyrene sulfonate) (PEDOT), polyaniline (PANI), and polypyrrole (PPy). Typically, PEDOT, one of the most widely used conductive polymers, exhibits sheet resistivities ranging from 10 to 500 Ω sq^{-1} depending on the processing conditions and doping levels.[58] Similarly, PANI and PPy generally possess R_s in the range of 100–10000 Ω sq^{-1}[59] and 100–1000 Ω sq^{-1},[60] respectively. In contrast, the sheet resistivity of the AuNP/2VP-EGDMA-PETT samples is <1 Ω sq^{-1}. These values of R_s underscore the effectiveness of this lithographic approach towards creating T/C patterns.

3. Conclusions

In this study, we have demonstrated an approach to fabricating T/C polymer-AuNP composites by combining HP, the GTGFRP, and templated, in situ AuNP formation. The resulting materials exhibited exceptional performance, with R_s of 0.42 Ω sq^{-1} at 100 mA, while maintaining high transmittance from 500 to 800 nm. These properties make these AuNP composites highly suitable for next-generation flexible electronics, sensors, and optical detection devices. HP utilizes a microfluidic-based approach for high-throughput materials discovery, enabling the screening of hundreds to thousands of reaction conditions on a single substrate, which can then be translated into other fabrication processes. Our approach allows for precise control over the polymer brush h and composition, enabling the systematic exploration of growth conditions and metal-binding capabilities, and here >9000 different printing conditions were tested to

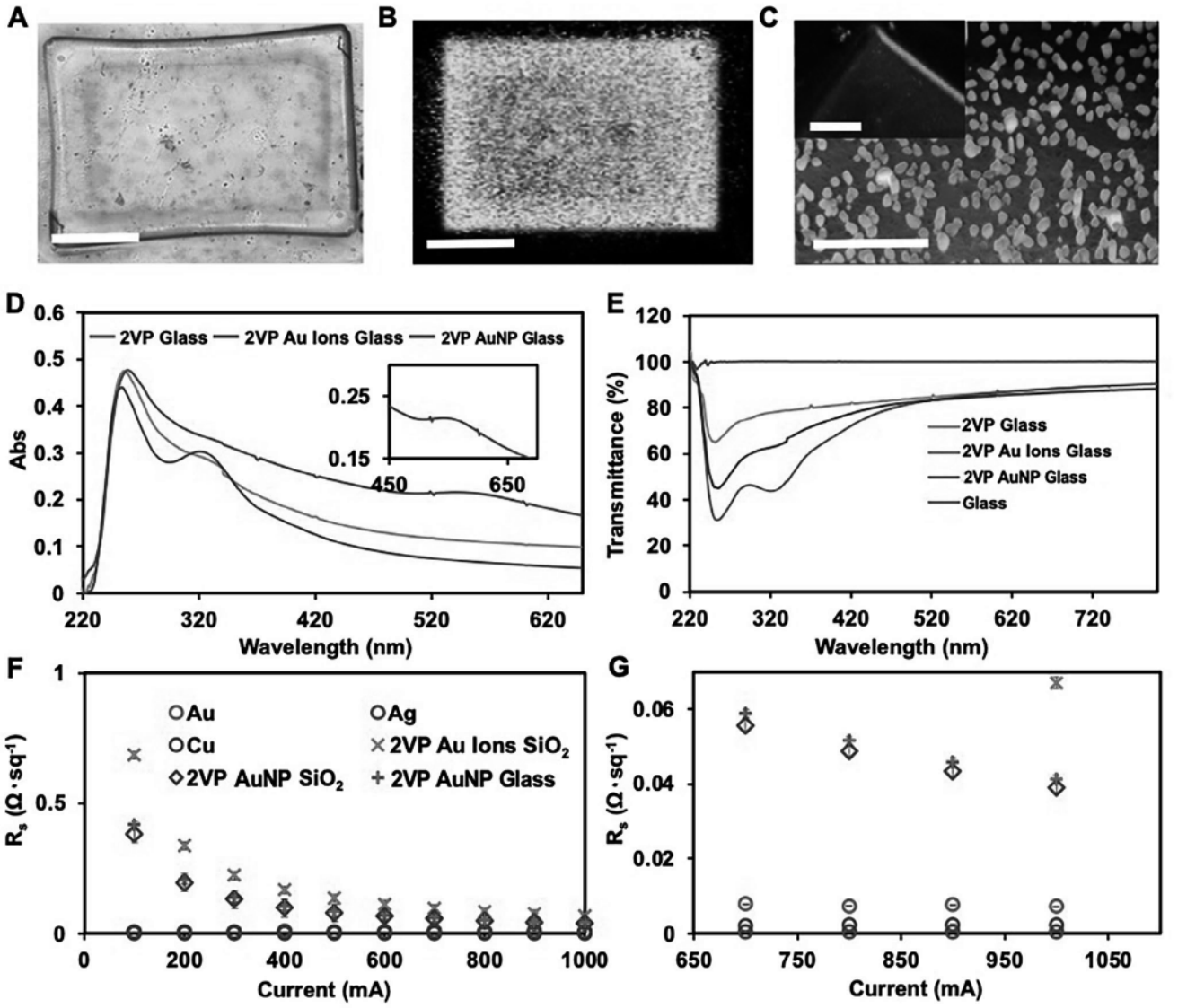

Figure 4. A) Optical image of 2VP-EGDMA-PETT polymer brushes bound to AuNPs prepared via in situ reduction on a thiol-functionalized glass surface passivated with maleic anhydride. Scale bar is 900 µm. B) Raman map (λ_{ex} = 532 nm) of peaks corresponding to Au (310–350 cm^{-1}) of 2VP-EGDMA-PETT polymer brushes with intercalated AuNPs. Scale bar is 1000 µm. C) SEM Image of 2VP-EGDMA-PETT polymer brushes bound to AuNPs patterned on a thiol-functionalized glass surface. Scale bar is 1 µm. Inset is SEM/EDS image of Au Mα1 intensity (green). Inset scale bar is 25 µm. D) UV–Vis Absorbance spectrum of 2VP-EGDMA-PETT polymer brushes patterned on a thiol-functionalized glass surface. (E) Transmittance data taken from the samples in (D). F) Sheet resistance (R_s) versus current (I) plot of different samples measured by a 4-point probe device. G) Expansion of plot in (F) showing R_s from I = 650–1050 mA.

achieve this control. By integrating AuNPs uniformly into the polymer matrix, we overcame common challenges such as poor adhesion and low conductivity that are typically associated with polymer-based conductive films. The grafted-from polymer brushes are covalently attached to the substrate, ensuring that these patterns maintain strong, stable interfaces even under various processing conditions. Our findings demonstrate that embedding AuNPs within the polymer brush matrix facilitates the formation of conductive pathways; however, the exact mechanisms underlying charge transport in these nanostructures have yet to be fully understood and is the subject of ongoing studies. The relationship between polymer brush height and key properties such as transparency and conductivity remains an important area for further exploration. Given the complex interplay between brush height, NP loading, and optical/electrical performance, future work will focus on systematically investigating how variations in brush height influence these properties. Understanding these correlations will provide deeper insights into the design space of polymer brush-based T/C films and enable further optimization for applications requiring precise control over optical and electrical performance. This work opens new possibilities for the scalable production of high-performance, T/C materials, with significant potential for application in wearable electronics, flexible displays, and implantable sensors.

Supporting Information

Supporting Information is available from the Wiley Online Library or from the author.

Acknowledgements

A.B.B. gratefully acknowledges financial support from Air Force Office of Scientific Research (FA9550-23-1-0230, FA9550-22-1-0513), Army Research Office (W911NF-23-1-0234), and National Science Foundation (DBI-2032176). K.L.M. gratefully acknowledges financial support from the National Science Foundation (Phase II CREST Center for Interface Design and Engineered Assembly of Low-dimensional Systems (IDEALS II), EES-2112550). A.R.C. gratefully acknowledges the support from the CUNY Llewllyn Fellowship. M.A.S. gratefully acknowledges financial support from the National Science Foundation Research Traineeship (NRT0 NanoBioNYC Program under Grant DGE-2151945). I.K. gratefully acknowledges financial support from the National Science Foundation (LEAP-HI 2245265). XPS and ToF-SIMS were collected at the CUNY ASRC Surface Science Facility. The authors thank Dr. Tai-De Li for assistance in collecting the data. The authors thank Dr. Tong Wang and Dr. Sheng Zhang at the CUNY ASRC Imaging Facility for their help in acquiring the SEM/EDS spectral data.

Conflict of Interest

The authors declare no conflict of interest.

Data Availability Statement

The data that supports the findings of this study are available in the Supporting Information of this article.

Keywords

Au-nanoparticles, bottom-up lithography, polymer brushes, transparent conductive films

Received: February 13, 2025
Published online:

[1] a) J. Miao, T. Fan, *Carbon*. **2023**, *202*, 495; b) J. Linnet, A. R. Walther, C. Wolff, O. Albrektsen, N. A. Mortensen, J. Kjelstrup-Hansen, *Opt. Mater. Express*. **2018**, *8*, 1733; c) M. Heydari Gharahcheshmeh, M. M. Tavakoli, E. F. Gleason, M. T. Robinson, J. Kong, K. K. Gleason, *Sci. Adv.* **2019**, *5*, 0414; d) S. A. Abbasi, Z. Chai, A. Busnaina, *Adv. Mater. Interfaces*. **2019**, *6*, 1900898.

[2] S. K. Maurya, H. R. Galvan, G. Gautam, X. Xu, *Energies*. **2022**, *15*, 8698.

[3] Z. Chen, S. Yang, J. Huang, Y. Gu, W. Huang, S. Liu, Z. Lin, Z. Zeng, Y. Hu, Z. Chen, B. Yang, X. Gui, *Nano-Micro Lett*. **2024**, *16*, 92.

[4] X. Feng, X. Wang, B. Zhang, J. Gu, C. Xu, S. Zhang, *J. Mater. Sci.: Mater. Electron*. **2022**, *33*, 25939.

[5] A. K. Mohammad, A. Garrod, A. Ghosh, *J. Build. Eng*. **2023**, *79*, 107950.

[6] a) X.-R. Zhang, H.-T. Deng, X. Zeng, Y.-L. Wang, P. Huang, X.-S. Zhang, *Nano Res.* **2024**, *17*, 4288; b) Y. Wan, C. Wang, B. Zhang, Y. Liu, H. Yang, F. Liu, J. Xu, S. Xu, *Sensors*. **2024**, *24*, 3799.

[7] a) W. A. D. M. Jayathilaka, K. Qi, Y. Qin, A. Chinnappan, W. Serrano-García, C. Baskar, H. Wang, J. He, S. Cui, S. W. Thomas, S. Ramakrishna, *Adv. Mater.* **2019**, *31*, 1805921; b) D. Sengupta, A. G. P. Kottapalli, *Adv. Electron. Mater.* **2024**, *10*, 2300436; c) Q. Shi, B. Dong, T. He, Z. Sun, J. Zhu, Z. Zhang, C. Lee, *InfoMat*. **2020**, *2*, 1131.

[8] A. Ramasubramaniam, R. Selhorst, H. Alon, M. D. Barnes, T. Emrick, D. Naveh, *J. Mater. Chem. C*. **2017**, *5*, 11158.

[9] D. J. Valles, Y. S. Zholdassov, A. B. Braunschweig, *Polym. Chem*. **2021**, *12*, 5724.

[10] a) C. Chen, Y. Zhao, W. Wei, J. Tao, G. Lei, D. Jia, M. Wan, S. Li, S. Ji, C. Ye, *J. Mater. Chem. C*. **2017**, *5*, 2240; b) M. Sajid, F. S. Awan, M. Javed, Z. J. Khattak, G. Hussain, S. F. Shah, K. Rahman, M. Saleem, *Lasers Manuf. Mater. Process*. **2023**, *10*, 276.

[11] X. Zhang, J. Lai, T. Gray, *Oxford Open Mater. Sci*. **2023**, *3*, https://doi.org/10.1093/oxfmat/itad010.

[12] T. O. L. Sunde, E. Garskaite, B. Otter, H. E. Fossheim, R. Sæterli, R. Holmestad, M.-A. Einarsrud, T. Grande, *J. Mater. Chem*. **2012**, *22*, 15740.

[13] S. K. Pradhan, E.-P. Kwon, L. J. Kweon, M.-S. Oh, *Mater. Today Commun*. **2024**, *41*, 110619.

[14] S. Lee, E. M. Leung, M. A. Badshah, A. A. Strzelecka, A. A. Gorodetsky, *APL Bioeng*. **2024**, *8*, 046101.

[15] K. Xie, A. Glasser, S. Shinde, Z. Zhang, J. M. Rampnoux, A. Maali, E. Cloutet, G. Hadziioannou, H. Kellay, *Adv. Funct. Mater*. **2021**, *31*, 21.

[16] P. Kowol, S. Bargmann, P. Görrn, J. Wilmers, *Appl. Mech*. **2023**, *4*, 514.

[17] a) C. W. Pester, H.-A. Klok, E. M. Benetti, *Macromolecules*. **2023**, *56*, 9915; b) M. Fromel, M. Li, C. W. Pester, *Macromol. Rapid Commun*. **2020**, *41*, 2000177.

[18] D. Boyaciyan, L. Braun, O. Löhmann, L. Silvi, E. Schneck, R. von Klitzing, *J. Chem. Phys*. **2018**, *149*, 163322.

[19] L. Jiang, X. Wang, L. Chi, *Small*. **2011**, *7*, 1309.

[20] S. Edmondson, V. L. Osborne, W. T. S. Huck, *Chem. Soc. Rev*. **2004**, *33*, 14.

[21] a) C. W. Pester, J. E. Poelma, B. Narupai, S. N. Patel, G. M. Su, T. E. Mates, Y. Luo, C. K. Ober, C. J. Hawker, E. J. Kramer, *J. Polym. Sci., Part A: Polym. Chem*. **2016**, *54*, 253; b) J. E. Poelma, B. P. Fors, G. F. Meyers, J. W. Kramer, C. J. Hawker, *Angew. Chem*. **2013**, *125*, 6982; c) M. Li, M. Fromel, D. Ranaweera, S. Rocha, C. Boyer, C. W. Pester, *ACS Macro Lett*. **2019**, *8*, 374; d) J. O. Zoppe, N. C. Ataman, P. Mocny, J. Wang, J. Moraes, H.-A. Klok, *Chem. Rev*. **2017**, *117*, 1105.

[22] A. M. Wong, D. J. Valles, C. Carbonell, C. L. Chambers, A. Y. Rozenfeld, R. W. Aldasooky, A. B. Braunschweig, *ACS Macro Lett*. **2019**, *8*, 1474.

[23] a) A. Kiełbasa, K. Kowalczyk, K. Chajec-Gierczak, J. Bała, S. Zapotoczny, *Polym. Adv. Technol*. **2024**, *35*, 6397; b) E. L. Foster, A. C. C. de Leon, P.-F. Cao, E. B. Caldona, R. C. Advincula, *Thin Solid Films*. **2022**, *758*, 139453.

[24] H. Kim, A. Piqué, J. S. Horwitz, H. Mattoussi, H. Murata, Z. H. Kafafi, D. B. Chrisey, *Appl. Phys. Lett*. **1999**, *74*, 3444.

[25] H. Aguilar-Bolados, M. Yazdani-Pedram, E. Quinteros-Jara, Q. Cuenca-Bracamonte, R. Quijada, J. Carretero-González, F. Avilés, M. A. Lopez-Manchado, R. Verdejo, *Polym. Test*. **2021**, *93*, 106986.

[26] G. D. Fu, J. P. Zhao, Y. M. Sun, E. T. Kang, K. G. Neoh, *Macromolecules*. **2007**, *40*, 2271.

[27] a) C. Park, J. Yoon, E. L. Thomas, *Polymer*. **2003**, *44*, 6725; b) C. J. Hawker, T. P. Russell, *MRS Bull*. **2005**, *30*, 952.

[28] G. Shalom, M. Christian, S.-S. Natalie, W. B. Dag, P. R. Christopher, W. A. Jens, T. Richard, A. J. J. René, M. N. Martin, S. Paul, S. Henning, *Nat. Mater*. **2006**, *5*, 950.

[29] M. I. Alonso, M. Campoy-Quiles, in *Ellipsometry of Functional Organic Surfaces and Films*, Vol. *52* (Eds: K. Hinrichs, K. J. Eichhorn), Springer Series in Surface Sciences, Switzerland **2018**, p. 335.

[30] P. Singh, K. Kumari, V. K. Vishvakrma, G. K. Mehrotra, R. Chandra, D. Kumar, R. Patel, V. V. Shahare, in *Green Technologies and Environmental Sustainability* (Eds: R. Singh, S. Kumar), Springer International Publishing AG, Cham, Switzerland **2017**, pp. 309–337.

[31] J.-Y. Kim, C.-R. Hwang, S.-H. Jo, W.-G. Jung, *Appl. Phys. Lett.* **2011**, *99*, 233304.
[32] L. Q. Pham, J. H. Sohn, C. W. Kim, J. H. Park, H. S. Kang, B. C. Lee, Y. S. Kang, *J. Colloid Interface Sci.* **2012**, *365*, 103.
[33] S. B. Aziz, Z. H. Z. Abidin, A. K. Arof, *Phys. B.* **2010**, *405*, 4429.
[34] N. Ferrer-Anglada, M. Kaempgen, V. Skákalová, U. Dettlaf-Weglikowska, S. Roth, *Diamond Relat Mater.* **2004**, *13*, 256.
[35] L. Zhang, T. Song, L. Shi, N. Wen, Z. Wu, C. Sun, D. Jiang, Z. Guo, *J. Nanostruct. Chem.* **2021**, *11*, 323.
[36] A. Elschner, W. Lövenich, *MRS Bull.* **2011**, *36*, 794.
[37] D. Bellet, M. Lagrange, T. Sannicolo, S. Aghazadehchors, V. H. Nguyen, D. P. Langley, D. Muñoz-Rojas, C. Jiménez, Y. Bréchet, N. D. Nguyen, *Materials.* **2017**, *10*, 570.
[38] T. Thirugnanasambandan, in *Environmental Nanotechnology*, Vol. *2*, (Eds: N. Dasgupta, S. Ranjan, E. Lichtfouse), Springer International Publishing, Cham, Switzerland **2019**, pp. 213–254.
[39] T.-W. Kang, S. H. Kim, C. H. Kim, S.-M. Lee, H.-K. Kim, J. S. Park, J. H. Lee, Y. S. Yang, S.-J. Lee, *ACS Appl. Mater. Interfaces.* **2017**, *9*, 33129.
[40] Y.-F. Li, X. Liu, J. Feng, Y. Xie, F. Zhao, X.-L. Zhang, Q. Pei, H.-B. Sun, *Nanophotonics.* **2020**, *9*, 3567.
[41] a) W. Sha, H. Wang, F. Guo, *J. Mater. Sci.* **2022**, *57*, 5346; b) S. Wang, Z. Wang, J. Li, L. Li, W. Hu, *Mater. Chem. Front.* **2020**, *4*, 692.
[42] K. A. Altammar, *Front. Microbiol.* **2023**, *14*, 1155622.
[43] J. Siegel, O. Lyutakov, V. Rybka, Z. Kolská, V. Švorčík, *Nanoscale Res. Lett.* **2011**, *6*, 96.
[44] C. D. Hodgman, *Hanbook of Chemistry and Physics: A Ready-Reference Book of Chemical and Physical Data*, CRP Press, Cleaveland, OH **1949**.
[45] T. Nishimura, N. Ito, K. Kinoshita, M. Matsukawa, Y. Imura, T. Kawai, *Small.* **2020**, *16*, 1903365.
[46] C. Carbonell, D. Valles, A. M. Wong, A. S. Carlini, M. A. Touve, J. Korpanty, N. C. Gianneschi, A. B. Braunschweig, *Nat. Commun.* **2020**, *11*, 1244.
[47] D. J. Valles, Y. S. Zholdassov, J. Korpanty, S. Uddin, Y. Naeem, D. R. Mootoo, N. C. Gianneschi, A. B. Braunschweig, *Angew. Chem.* **2021**, *133*, 20513.
[48] Y. S. Zholdassov, D. J. Valles, S. Uddin, J. Korpanty, N. C. Gianneschi, A. B. Braunschweig, *Adv. Mater.* **2021**, *33*, 2100803.
[49] J. Chai, F. Huo, Z. Zheng, L. R. Giam, W. Shim, C. A. Mirkin, *Proc. Natl. Acad. Sci. USA.* **2010**, *107*, 20202.
[50] D. J. Valles, Y. Naeem, A. Y. Rozenfeld, R. W. Aldasooky, A. M. Wong, C. Carbonell, D. R. Mootoo, A. B. Braunschweig, *Faraday Discuss.* **2019**, *219*, 77.
[51] a) L. Bonda, D. J. Valles, T. L. Wigger, J. Meisner, A. B. Braunschweig, L. Hartmann, *Macromolecules.* **2023**, *56*, 5512; b) M. I. Feldhof, S. Sperzel, L. Bonda, S. Boye, A. B. Braunschweig, U. I. M. Gerling-Driessen, L. Hartmann, *Chem. Sci.* **2024**, *15*, 16768.
[52] a) L. Huang, P.-C. Chen, M. Liu, X. Fu, P. Gordiichuk, Y. Yu, C. Wolverton, Y. Kang, C. A. Mirkin, *Proc. Natl. Acad. Sci. USA.* **2018**, *115*, 3764; b) M. Behera, S. Ram, *Appl. Nanosci.* **2013**, *3*, 83; c) J. E. Millstone, S. J. Hurst, G. S. Métraux, J. I. Cutler, C. A. Mirkin, *Small.* **2009**, *5*, 646; d) J. Hong, J. Xie, S. Mirshahghassemi, J. Lead, *RSC Adv.* **2020**, *1*, 3266; e) J. Liu, Z. Zeng, X. Cao, G. Lu, L.-H. Wang, Q.-L. Fan, W. Huang, H. Zhang, *Small.* **2012**, *8*, 3517.
[53] E. Çakmakçi, B. Yuce-Dursun, S. Demir, *React. Funct. Polym.* **2017**, *111*, 38.
[54] P. J. Murphy, G. Stevens, M. S. LaGrange, *Geochim. Cosmochim. Acta.* **2000**, *64*, 479.
[55] P. Kareem, Y. Kwon, Y. Shin, *IEEE Trans. Semicond. Manuf.* **2020**, *33*, 283.
[56] C. A. Schneider, *Nat. Methods.* **2012**, *9*, 671.
[57] a) P. K. Ngumbi, S. W. Mugo, J. M. Ngaruiya, *IOSR J. Appl. Chem.* **2018**, *11*, 25; b) W. Haiss, N. T. K. Thanh, J. Aveyard, D. G. Fernig, *Anal. Chem.* **2007**, *79*, 4215.
[58] S.-P. Rwei, Y.-H. Lee, J.-W. Shiu, R. Sasikumar, U.-T. Shyr, *Polymers.* **2019**, *11*, 134.
[59] a) N. Sharma, A. Singh, N. Kumar, A. Tiwari, M. Lal, S. Arya, *J. Mater. Sci.* **2024**, *59*, 6206; b) L. Wei, Q. Chen, Y. Gu, *Synth. Met.* **2010**, *160*, 405.
[60] A. Dianatdar, M. Miola, O. De Luca, P. Rudolf, F. Picchioni, R. K. Bose, *J. Mater. Chem. C.* **2022**, *1*, 557.